HHS Public Access

Author manuscript

Mol Imaging Biol. Author manuscript; available in PMC 2021 April 01.

Published in final edited form as:

Mol Imaging Biol. 2020 April ; 22(2): 384–396. doi:10.1007/s11307-019-01382-x.

Evaluating the Role of Amide-Proton-Transfer (APT) Weighted Contrast, Optimized for Normalization and Regions of Interest Selection, in Differentiation of Neoplastic and Infective Mass Lesions on 3T MRI

Ayan Debnath[1], **Rakesh Kumar Gupta**[2], **Anup Singh**[1,3]

[1]Centre for Biomedical Engineering, Indian Institute of Technology Delhi, India

[2]Fortis Memorial Research Institute, Gurgaon, India

[3]Department of Biomedical Engineering, All India Institute of Medical Sciences, India

Abstract

Purpose: To evaluate the role of Amide-proton-transfer weighted (APT-w) magnetic resonance imaging (MRI) in differentiating neoplastic and infective-mass-lesions using different contrast normalizations, region-of-interest (ROI) selection and histogram analysis.

Procedures: Retrospective study included thirty-two treatment-naive patients having intra-cranial-mass-lesions (ICMLs): low-grade-glioma (LGG) = 14, high-grade-glioma (HGG) =10, infective-mass-lesions = 8. APT-w MRI images were acquired along with conventional MRI images at 3T. APT-w contrast, corrected for B_0-field inhomogeneity, was computed and optimized with respect to different types of normalizations. Different ROIs on lesion region were selected followed by ROI analysis and histogram analysis. Statistical analysis was performed using Shapiro-Wilk's test, T-tests, ANOVA with Tukey's post-hoc test and receiver-operation-characteristics (ROC) analysis.

Results: ICMLs showed significantly ($p < 0.01$) higher APT-w contrast in lesion compared to contra-lateral side. There was a substantial overlap between mean APT-w contrast of neoplastic and infective-mass-lesions as well as among different groups of ICMLs irrespective of ROIs selection and normalizations. APT-w contrast (using Type-4 normalization: normalized with reference signal at negative offset-frequency and APT-w contrast in normal-appearing-white-matter) reduced variability of APT-w contrast across different subjects and overlap was less compared to other types of normalizations. There was a significant difference ($p < 0.05$) between

Corresponding author postal address: Dr. Anup Singh, Block-II, Room No. 299, Center for Biomedical Engineering, Indian Institute of Technology Delhi, New Delhi -110016, India, Tel:+91-11-2659-1055(O), anupsm@iitd.ac.in / anupsmri@gmail.com / anups.minhas@gmail.com.

Conflict of Interest

The authors declare that they have no conflict of interest.

neoplastic and infective-mass-lesions using T-test for different histogram parameters of Type-4 normalized APT-w contrast. ANOVA with post-hoc showed significant difference ($p < 0.05$) for different histogram parameters of APT-w contrast (Type-4 normalization) between LGG and HGG, LGG and infective-mass-lesion. Histogram parameters such as standard-deviation, mean-of-top-percentiles and median provided improved differentiation between neoplastic and infective-mass-lesions compared to mean APT-w contrast. A greater number of histogram parameters of Type-4 normalized APT-w contrast corresponding to active lesion region can significantly differentiate between ICMLs than other type of normalizations and ROIs.

Conclusions: APT-w contrast using Type-4 normalization and active lesion region (ROI-2) should be used for studying APT. APT-MRI should be combined with other MRI techniques to further improve the differential diagnosis of ICMLs.

Keywords

Chemical Exchange Saturation Transfer (CEST); Amide-proton-transfer-weighted; MRI; neoplastic mass lesions; infective mass lesions; intra cranial mass lesions

Introduction

Most of the pathological processes are initiated by abnormal changes in bio-molecular environment at the cellular level. *In vivo* and non-invasive detection of these bio-molecules is important for diagnosis and characterization of diseases. Due to low concentration of these labile molecules, *in vivo* detection of these molecules is not possible using conventional imaging [1]. Recently, chemical exchange saturation transfer (CEST) [2–6] has been proposed as a novel non-invasive magnetic resonance imaging (MRI) contrast mechanism for high-resolution mapping of molecular information in biological tissues. CEST contrast at an offset frequency of +3.5 ppm from water protons resonance, at low saturation RF power, has been reported [7] to be sensitive to amide protons of labile peptides and small proteins. This contrast is widely known as amide-proton-transfer (APT) contrast [7–9]. More specifically, this contrast has additional signal contributions from other multiple confounding molecules and thus appropriate nomenclature is amide-proton-transfer-weighted (APT-w) [10] contrast. APT-w MRI is sensitive to low-concentration of bio-molecules (endogenous cellular proteins and peptides) [11] and tissue physiochemical properties (pH and temperature) [8,12].

Preliminary studies have shown the potential applications of APT-MRI in stroke [12,13], central nervous system (CNS) lymphoma [14] and brain tumor grading [7,15–20]. Recently, one group has investigated APT-w contrast on lymphoma and compared with high grade tumor [14]. Infective mass lesions in the CNS such as tuberculoma (TB), neurocysticercosis (NCC), etc. are widely prevalent in developing countries and sometime behave similar to neoplastic mass lesions on conventional MRI. However, till date there are no studies available on APT-w imaging of infective mass lesions and its comparison with neoplastic mass lesions. Conventional MRI images like T_2-w, FLAIR, post contrast T_1-w (PCT_1-w) reveals the location and the appearance of lesions but does not provide enough knowledge about lesion classification. Standard MRIs along with other MRIs viz. dynamic contrast enhanced (DCE) MRI, diffusion MRI, magnetization transfer contrast though provide useful

information for detection of infective and neoplastic mass lesions, still, there are some challenges [21] in their differentiation. Therefore, potential of APT-w imaging in differentiating intra-cranial-mass-lesions (ICMLs) needs to be investigated.

Most of the reported studies [13, 14, 16, 19–21] have used magnetization transfer ratio (MTR) or CEST asymmetry ($CEST_{asym}$) to compute APT-w contrast. The conventional method of asymmetry analysis uses M_0 (signal intensity without radio-frequency (RF) saturation) for normalization. Some studies have suggested normalization by negative offset frequency ($M_{sat(-3.5ppm)}$ which is the signal intensity at −3.5ppm upfield from water resonating frequency (4.7 ppm which is considered as 0 ppm)) for increasing dynamic range of contrast [22]. Few studies reported normalization by mean APT-w contrast using normal appearing white matter (NAWM) [15,19] region for improved analysis. NAWM are regions on white matter with no visible hyperintensity on T_2-w, FLAIR and PCT_1-w images. Previous studies have used different types of normalizations in isolation. However, effect of different normalizations on APT-w contrast in terms of differentiation of ICMLs need to be evaluated. Regions-of-interest (ROIs) selection on lesion plays an important role, therefore, optimization for ROIs selection also needs to be carried out in terms of APT-w contrast's ability in differentiating ICMLs. Moreover, histogram analysis provides more insight to gain more information about lesion and thus might improve the diagnosis and grading [23–25].

We hypothesize that optimum normalization, ROIs selection and histogram analysis of APT-w contrast can improve differentiation of ICMLs. The purpose of this study was to investigate the potential of APT-w contrast in differentiating infective and neoplastic mass lesions and to determine the optimal combination using different types of normalizations, ROIs selection and histogram parameters for more sensitive detection of tumor against infection.

Materials and Methods

Patient Recruitment

MRI data of 32 treatment naive patients (24 males, 8 females; mean age 43 years; range 11–82 years) with ICMLs were included in this study. This retrospective study was approved by the institutional ethics committee, and informed consent was obtained from the patients.

MR Imaging Sequence and Protocols

All the MRI experiments were performed on 3T whole body Inginia MRI system (Philips Healthcare, The Netherlands) using a 15-channel head-neck coil for reception. MRI data included following images as a part of clinical protocol: T_1-w and T_2-w turbo-spin-echo (TSE); fluid-attenuated-inversion recovery (FLAIR); post contrast-enhanced T_1-w (PCT_1-w) images. The following parameters were used for T_2-w: echo train length (ETL) 16, repetition time (TR)/echo time (TE) 3500 ms/90 ms, field of view (FOV) 240×240 mm^2, matrix size 256×256, slice thickness 6mm, slices 12, flip angle 90°; T_1-w: ETL 4, TR/TE 360 ms/10 ms, FOV 240×240 mm^2, matrix size 256×256, slice thickness 6mm, slices 12, flip angle 70°; DWI: ETL 61, TR/TE 4096 ms/112 ms, FOV 243×230mm^2, matrix size 192×192, slice thickness 5 mm, slices 27, flip angle 90°, b = 0 and 1000; FLAIR: ETL 167,

TR/TE 4700 ms/290 ms, FOV 247×247 mm^2, matrix size 288×288, slice thickness 0.9 mm, slices 25, flip angle 90°, inversion recover (IR) time 1650 ms. For acquiring PCT_1-w images, 0.1mmol/kg body weight of gadobenate dimeglumine Gd-BOPTA (Multihance, Bracco) was administered with the help of power injector at rate of 3 ml/s followed by bolus injection of a 30 ml saline flush. PCT_1-w image was acquired after 2 min of contrast injection. The parameters for PCT_1-w images are ETL 55, TR/TE 700 ms/24 ms, FOV 250×250 mm^2, matrix size 560×560, slice thickness 0.9 mm, slices 25, flip angle 90°.

The APT-w MRI images were also acquired before the administration of the contrast agent [26]. The pulse sequence [27, 28] used to acquire APT-w MRI comprised of three sections: four blocks of radiofrequency saturation preparation pulses (each block with root mean square B_1 (B_{1rms}) of 2 μT and duration of 200 ms) each followed by a crusher gradient (saturation duration of 10ms and amplitude of 10mT/m); lipid suppression (flip angle 100° and duration of 17.6 ms) followed by a crusher gradient (saturation duration of 2ms and amplitude of 22mT/m) and readout. APT-w images were acquired for a single representative slice (2D acquisition), positioned at center of lesion, with 64 frequency points (± 0 Hz to ± 1792 Hz with step size of 64 Hz, and unsaturated image at 10,000Hz). Other imaging parameters were: ETL 42, TR/TE 3000 ms/5.54 ms, FOV 212×212 mm^2, matrix size 176×176, flip angle 90°. Fat suppression was achieved using SPIR. Total scan time for 2D APT-w images was 5.0 min. Water-Saturation-Shift-Referencing (WASSR) [29] data was also acquired for generating B_0 map, which is required for B_0 inhomogeneity correction of APT-w images. WASSR images were collected for the same slice with 26 frequency points (−192 to +192 Hz with a step size of 16 Hz) using saturation B_{1rms} of 0.5 μT and duration of 200ms.

Theory

Exchangeable solute protons of amide group were selectively saturated using RF irradiation. Due to exchange of protons, the saturation was transferred to bulk water and thus water signal reduced. For computing APT-w contrast, the present study used four types of normalizations:

Type-1: APT-w contrast when normalized with M_0(APT_{M_0}):

$$APT_{M_0} = \frac{M_{sat(-3.5ppm)} - M_{sat(+3.5ppm)}}{M_0} \times 100 \quad \ldots(i)$$

where $M_{sat(+3.5ppm)}$ and $M_{sat(-3.5ppm)}$ are the signal intensities with downfield and upfield of water resonating frequency.

Type-2: APT-w contrast when normalized with $M_{sat(-3.5ppm)}$ (APT_{Neg}):

$$APT_{Neg} = \frac{M_{sat(-3.5ppm)} - M_{sat(+3.5ppm)}}{M_{sat(-3.5ppm)}} \times 100 \quad \ldots(ii)$$

Type-3: APT-w contrast when normalized with M_0 and NAWM ($APT_{M_0\_NAWM}$):

$$APT_{M_0\_NAWM} = APT_{M_0} - M_1 \quad \ldots(iii)$$

where, M_1 is the mean value of APT_{M0}-w contrast in NAWM

Type-4: APT-w contrast when normalized with $M_{sat(-3.5ppm)}$ and NAWM (APT_{Neg_NAWM})

$$APT_{Neg\_NAWM} = APT_{Neg} - M_2 \quad \ldots(iv)$$

where, M_2 is the mean value of APT_{Neg}-w contrast in NAWM

Usually, MTR asymmetry or $CEST_{asym}$ analysis mitigates the effect of direct saturation (DS) and Magnetization Transfer (MT) with the assumption that DS and MT are symmetrical [30] around water resonating frequency. As such, for *in vivo* data, there is a small MT asymmetry effect, which confounds APT-w contrast. Along with this, relayed Nuclear-Overhauser-Effect (rNOE) effect also contaminates APT-w contrast using asymmetry analysis.

Image processing and analysis

All the data processing was performed using in house written programs in MATLAB R2014-R2017 (The MathWorks, Inc., MA, USA). The pre-processing steps included registration of APT-w, WASSR, T_2-w, PCT_1-w and FLAIR images with T_1-w images followed by automated de-scalping of APT-w images for background noise removal. The registration and de-scalping were carried out using SPM12 software. B_0 map was generated using WASSR methodology[29]. APT-w images at ± 3.5ppm (± 448 Hz) were corrected for B_0 inhomogeneity using neighborhood frequency offset data (± 320 Hz to ± 576Hz with step size of 64 Hz). Finally, APT-w maps were computed using Type-1, 2, 3, 4 normalization approaches as described in the previous section. In this study, single slice APT-w images were processed and analyzed.

ROIs selection and analysis

In-house devloped semi-automatic lesion segmentation approach based upon seeded region growing algorithm [31] and morphological operations was used to segment out different parts of lesion. Firstly, hyper-intense region or contrast enhancing region of PCT_1-w image was segmented out using region growing algorithm and this region corresponds to active lesion region (ROI-2). For non-enhancing lesions (n = 6), ROI-2 was selected by experienced radiologist on T_2-w image using polygon ROI selection in MATLAB R2017. Secondly, hyper-intense region on FLAIR image was segmented using same semiautomatic segmentation approach. Lastly, FLAIR hyper-intense mask was combined with contrast enhancing mask (ROI-2) to obtain entire lesion region (ROI-1). Contra-lateral regions of ROI-1 and ROI-2 (cROI-1 and cROI-2) were generated automatically using in-house developed MATLAB code. In addition, normal appearing white matter (NAWM) and normal appearing gray matter (NAGM) masks were also obtained using SPM-12 software with T_1-w images. Entire lesion region (ROI-1) was excluded from NAWM and NAGM followed by morphological operation erosion (kernel size −3×3) to obtain pure NAMW mask and NAGM mask and to remove contribution from partial volume effects.

Average APT-w contrast in NAWM was used to compute APT_{M0_NAWM} contrast using Type-3 normalization and APT_{Neg_NAWM} contrast using Type-4 normalization. Mean and standard deviation (SD) of APT-w contrast corresponding to different types of normalizations were computed from above mentioned ROIs. APT-w contrast was reported in the study as Mean ± SD. Box and whisker plots were also generated to provide a graphical representation of data distribution of APT-w contrast. Computed APT-w maps were color overlaid on anatomical images.

Histogram analysis

Histogram analysis [23–25] of APT-w contrast using Type-3 and Type-4 normalizations corresponding to ROI-1 and ROI-2 were carried out. Apart from mean and SD, the following histogram parameters were calculated: a) median, b) mode, c) kurtosis, d) skewness, e) entropy, f) full width at half maximum (FWHM), g) 10^{th}, 25^{th}, 50^{th}, 75^{th}, 90^{th} percentile (pr_10, pr_25, pr_50, pr_75 and pr_90), h) mean of the values greater than 10^{th}, 25^{th}, 50^{th}, 75^{th}, 90^{th} percentile (mtop10, mtop25, mtop50, mtop75, mtop90), i) standard deviations of the values greater than 10^{th}, 25^{th}, 50^{th}, 75^{th}, 90^{th} percentile (sdtop10, sdtop25, sdtop50, sdtop75, sdtop90).

Statistical analysis

Tests for normality was carried out for all the parameters of APT-w contrast extracted from both ROI-1 and ROI-2 using Shapiro-Wilk's test. This test was carried out for each group of ICMLs (low grade glioma (LGG), high-grade-glioma (HGG) and infective mass lesions) separately. After normality testing, mean, median, mode and other histogram parameters of APT-w contrast were compared between neoplastic mass lesion and infective mass lesion using Independent Student's T-test with two tails. Histogram parameters of APT-w contrast were also compared among different groups of ICMLs (LGG, HGG and infective mass lesions) using a One-way analysis of variance (ANOVA) with Tukey's honestly significant difference (HSD) post-hoc test. While differentiating lesion from contra-lateral region, Independent Student's T-test was used. The difference was considered statistically significant if $p<0.05$. Receiver operation characteristics (ROC) analysis was conducted to evaluate the diagnostic performance of the histogram parameters in differentiating neoplastic from infective mass lesion, as well as in differentiating ICMLs. Sensitivity, specificity, area under curve (AUC) with 95% confidence interval (CI), accuracy and cut off were computed in ROC analysis. Statistical analysis was performed with a commercially available software package SPSS.v.15 (IBM SPSS Statistics, v. 15.0; Armonk, NY).

Results

Pathological diagnosis

A total of 24 neoplastic mass lesions and 8 infective mass lesions were include in this study. Neoplastic mass lesion includes 14 low grade glioma (LGG) (Pilocytic Astrocytoma = 6, WHO grade I; Ganglioglioma = 1, WHO grade I; Astrocytoma = 5, WHO grade II; Oligodendroglioma = 2, WHO grade II) and 10 high grade glioma (HGG) (Anaplastic Astrocytoma = 4, WHO grade III; Anaplastic Oligoastrocytoma = 1, WHO grade III;

Ganglioglioma = 1, WHO grade III; Glioblastoma (GBM) = 4, WHO grade IV). Infective mass lesion includes 8 patients (TB = 3, Tubercular abscess = 1, Aspergillus granuloma =1, NCC = 3).

APT-w contrast measurement by different normalizations

Infective and neoplastic mass lesions in the current study showed significantly ($p < 0.01$) higher APT-w contrast compared to its contra-lateral side (Fig. 1, Fig. 2). For all types of normalizations, APT-w contrast corresponding to ROI-1 and ROI-2 were significantly ($p < 0.01$) higher compared to cROI-1 and cROI-2 respectively. In general, it was found that mean APT-w contrast in NAWM regions is lower than APT-w contrast in NAGM for all types of normalizations (Suppl. Fig. 1, see Electronic Supplementary Material (ESM)). Suppl. Fig. 1 shows APT_{M0_NAWM} contrast (Type-3 normalization) and APT_{Neg_NAWM} contrast (Type-4 normalization) has higher dynamic range and smaller inter-quartile range than APT_{M0} contrast (Type-1 normalization) and APT_{Neg} contrast (Type-2 normalization). Supplementary Fig. 1c and d shows that median has been shifted to the center of box plots, which indicate symmetry in distribution of the data. Figure 1 shows necrotic region with hypointense APT-w contrast compared to active tumor. It shows APT-w maps can clearly differentiate necrotic or cystic regions from active lesions. The APT-w maps show a difference in contrast between WM, GM and intracranial lesions. Figure 2 shows that variability for NAWM and NAGM across different subjects was reduced in APT_{M0_NAWM} contrast (column 8) and APT_{Neg_NAWM} contrast (column 9); whereas variability for NAWM and NAGM tissues across different subjects were more in APT_{M0} contrast (column 6) and APT_{Neg} contrast (column 7). Supplementary Fig. 2 (see ESM) shows the selections of ROIs on a representative case of LGG.

The box and whisker plots in Fig. 3 show that there is a substantial overlap of mean APT-w contrast of neoplastic and infective mass lesions for all types of normalizations corresponding to ROI-1 and ROI-2. The mean APT_{M0} contrast (Type-1 normalization) and APT_{Neg} contrast (Type-2 normalization) for neoplastic mass lesions were 1.35 ± 0.98% and 2.21 ± 1.69% (for ROI-1), 1.53 ± 1.16% and 2.52 ± 1.98% (for ROI-2) respectively. The mean APT_{M0} contrast (Type-1 normalization) and APT_{Neg} contrast (Type-2 normalization) for infective mass lesions were 1.31 ± 0.62% and 2.35 ± 1.15% (for ROI-1), 1.71 + 0.83% and 3.09 + 1.53% (for ROI-2). This showed that mean APT-w contrast is higher in Type-2 than Type-1 normalization.

The box and whisker plots (Fig. 4) provide comparison of average APT-w contrast for different groups of ICMLs, using Type-1,2,3,4 normalizations, corresponding to ROI-1 and ROI-2. For all kinds of ROIs and normalizations, there is a substantial overlap among mean APT-w contrast of LGG, HGG and infective-mass-lesions. The mean APT_{M0} contrast (Type-1 normalization) is lower than APT_{Neg} contrast (Type-2 normalization) for all ICMLs corresponding to ROI-1and ROI-2. The mean APT-w contrast for HGG is higher than LGG for all types of normalizations and ROIs. The APT-w contrast corresponding to Type-4 normalization and ROI-2 for LGG was 3.58 ± 0.65 and HGG was 5.14 ± 0.811.

Statistical analysis (Shapiro-Wilk's: Test for normality)

Normality test showed that the data sets considered in this study were normally distributed. A Shapiro-Wilk's test ($p > 0.05$) showed that mean APT_{Neg_NAWM} contrast (Type-4 normalization) corresponding to ROI-2 were normally distributed for LGG [p-value = 0.36, skewness = −0.18 (standard error (SE) = 0.59), kurtosis = −1.37(SE = 1.15)], HGG [p-value = 0.12, skewness = 0.91 (SE = 0.69), kurtosis = 0.83 (SE = 1.33)] and infection [p-value = 0.79, skewness = 0.81(SE = 0.75), kurtosis = 0.31(SE = 1.48)]. Similarly, other histogram parameters also showed normal distributions for all types of normalized APT-w contrast.

Statistical analysis (T-test)

Table 1 shows only those histogram parameters which can significantly differentiate ($p < 0.05$) between neoplastic and infective mass lesions using independent Student's T-test. Mean of APT-w contrast for Type-1, Type-2 and Type-3 normalizations showed insignificant difference between neoplastic and infective mass lesions for all ROIs. The mean APT_{Neg_NAWM} contrast (Type-4 normalization) can significantly differentiate ($p < 0.05$) neoplastic from infective mass lesions for ROI-2 (Table-1) and not for ROI-1. While comparing histogram parameters of APT-w contrast corresponding to ROI-1 and ROI-2, a greater number of histogram parameters can significantly differentiate ($p<0.05$) neoplastic from infective mass lesions corresponding to ROI-2 considering Type-4 normalization (Table-1). Similar number of histogram parameters can significantly differentiate ($p<0.05$) between neoplastic and infective mass lesions for ROI-1 and ROI-2 considering Type-3 normalization. While comparing histogram parameters of APT-w contrast corresponding to Type-3 and Type-4 normalizations, a greater number of histogram parameters of Type-4 than Type-3 normalizations can significantly differentiate ($p<0.05$) between neoplastic and infective mass lesions for both ROI-1 and ROI-2.

Statistical analysis (ANOVA with post-hoc test)

Table-2 demonstrates histogram parameters which can significantly differentiate ICMLs using one-way ANOVA test. Mean of APT-w contrast for Type-1, Type-2 and Type-3 cannot significantly differentiate different group of ICMLs for both ROI-1 and ROI-2. Only mean of APT_{Neg_NAWM} contrast (Type-4 normalization) corresponding to ROI-2 can significantly differentiate ($p < 0.05$) among different group of ICMLs. There were a greater number of histogram parameters for Type-4 normalization corresponding to ROI-2 which provide significance difference ($p < 0.05$) among ICMLs. One-way ANOVA with Tukey's HSD post-hoc test showed a significant difference ($p < 0.05$) between LGG and infection for different histogram parameters of Type-4 normalizations corresponding to ROI-2. The mode of Type-4 normalization provided significant difference ($p < 0.05$) between LGG and HGG corresponding to ROI-2. The Skewness of Type-3 normalization can significantly differentiate ($p < 0.05$) HGG from infection corresponding to ROI-1. The mean, SD, median, mtop10, mtop25, mtop50, mtop75 and mtop90 of Type-4 normalization provided significant difference ($p<0.05$) between neoplastic and infective mass lesions corresponding to ROI-2.

ROC analysis

The present study shows ROC analysis of those histogram parameters which provided significant difference in distinguishing neoplastic from infective mass lesions as well as in between different group of ICMLs. Table-3 shows ROC analysis of different histogram parameters for Type-4 normalization corresponding to ROI-2 to distinguish neoplastic from infective mass lesions. Figure 5 demonstrate ROC analysis of mean of Type-4 (Fig. 5a) normalized APT-w contrast considering ROI-2 to differentiate between neoplastic and infective mass lesions. In the discrimination between neoplastic and infective mass lesions using mean of Type-4 normalization corresponding to ROI-2, a sensitivity and a specificity of 50% and 80% respectively were observed with accuracy of 72% and AUC was 65%, when a cut-off value of 5.3% was applied. Figure 5b and Table 4 shows ROC analysis of APT_{Neg_NAWM} contrast (Type-4 normalization) corresponding to ROI-2 in distinguishing LGG from infective mass lesions. ROC analysis provided a sensitivity of 62.5%, a specificity of 71.43%, AUC of 73.21%, accuracy of 68.18%, and cut-off value 4.77% in distinguishing between LGG and infective mass lesions.

All the percentile parameters (pr_10, pr_25, pr_50, pr_75 and pr_90) and mean of top-percentiles (mtop10, mtop25, mtop50, mtop75, mtop90) provided significant difference ($p<0.05$) simultaneously. Therefore, only mtop10, mtop25, mtop50, mtop75, mtop90 were mentioned in tables. The mean of values greater than top percentiles of Type-3 and Type-4 normalized APT-w contrast were higher in HGG than LGG considering ROI-1 and ROI-2. The SD of APT_{M0_NAWM} contrast (Type-3 normalization) corresponding to ROI-2 were 0.42 and 0.55 in LGG and HGG respectively; whereas, SD of APT_{Neg_NAWM} contrast (Type-4 normalization) corresponding to ROI-2 were 0.65 and 0.81 in LGG and HGG respectively. It showed that SD of APT-w contrast was higher in HGG than LGG. FWHM of APT_{Neg_NAWM} contrast (Type-4 normalization) corresponding to ROI-2 were 0.59 and 0.96 for LGG and HGG respectively. Table 1 to Table 4 showed histogram parameters in details.

Discussion

The present study demonstrates that APT-w contrast were significantly higher in ICMLs compared to the contra-lateral region, NAWM and NAGM. Similar findings were reported in previous studies[16] on tumor tissues, which mentioned increase in APT-w contrast in lesion regions compared to normal tissue regions. This occurs due to increased cellular protein and peptide contents in lesion regions. The smaller inter-quartile range in the box plots of Type-3 and Type-4 normalizations resulted in reducing the inter-subject variability of APT-w contrast in both WM and GM tissues. Results of the current study agree with those reported by Wen, et. al. [11] and other studies [32], demonstrating that the average APT-w contrast was significantly lower in the necrotic or cystic region compared to healthy contra-lateral region. This can be linked with biological characteristics of the lesion. Higher endogenous mobile protein and peptide concentration is found in active lesion than necrotic regions.

One of the main purpose of the current study was to evaluate the role of different APT normalizations for differentiating neoplastic and infective mass lesions as well as ICMLs. In the present study, it was observed that mean APT-w contrast, using all types of normalizations, was higher in HGG compared to LGG but statistical difference was non-

significant ($p > 0.05$). Our results are in line with previous studies [15,33] which observed a similar trend due to higher concentration of proteins and peptides in HGG compared to LGG. HGG has higher micro-vasculature than LGG which reflects in higher APT-w contrast in HGG compared to LGG. Previously reported study [19] has also shown that there was a non-significant difference between LGG and HGG. Recent study by Togao, et. al. [15] showed that there was no strict threshold value in grading of tumors, APT-w contrast was around 2 in grade-II, 3 in grade-III, 4 in grade-IV. The current study could not find significant difference among ICMLs (like LGG and infection) if we consider Type-1 and Type-2 normalizations, but there was significant difference among them considering Type-3 and Type-4 normalizations for the same ROI-2. This might be due to the internal normalization, which reduces variability among different subjects and hence improves differentiation. Type-2 normalization increases the dynamic range of $CEST_{asym}$ contrast compared to Type-1 normalization[21]. Thus, mean APT-w contrast is always higher in Type-2 than Type-1 normalizations. One point that is noteworthy to mention is that contra-lateral ROIs were not used for any kind of normalizations used in this study because contra-lateral ROIs may involve WM and GM with significantly different contrast variability. APT-w contrast showed less variability in NAWM, therefore average value in this tissue was used for normalization. Type-3 and Type-4 normalizations used NAWM reference region, which decreased variability among subjects and hence improved the differentiation of ICMLs [33]. APT-w contrast which were normalized with NAWM i.e. APT_{M0_NAWM} contrast (Type-3 normalization) and APT_{Neg_NAWM} contrast (Type-4 normalization) can be used as a bio-markers for differentiation between neoplastic and infective mass lesions [34]. In the current study, APT-w contrast in NAWM were negative; therefore, Type-3 and Type-4 normalizations resulted in an increase in values compared to Type-1 and Type-2 normalizations. Different type of normalizations provides a comprehensive view and better degree of freedom to compute APT-w contrast, which improves differentiation of ICMLs.

Placement of ROIs plays a crucial role in differentiating ICMLs. Manual selection of ROIs [35,36] is subjective and can lead to substantial variation in measurements, hampering the reliability of histogram and statistical analysis. Thus, in the current study a semiautomatic approach was adopted for ROI selection to reduce subjectivity or bias. The combination of seeded region growing algorithm followed by morphological operations has been implemented in the current study for semi-automated ROI selection process. NAWM and NAGM masks were generated using SPM-12 software might be erroneous, particularly for images having large size lesions. Thus, to obtain pure NAWM and pure NAGM, entire lesion mask regions was subtracted from NAWM and NAGM masks.

Histogram analysis of APT-w contrast has been used to grade cerebral tumors [23–25]. We considered histogram analysis of Type-3 and Type-4 normalized APT-w contrast because normalizations with NAWM decreases the variabilities between subjects. Histogram analysis has been carried on both ROI-1 and ROI-2 because ROI-1 takes care of the entire lesion (active-tumor along with necrosis/cystic and edema) whereas ROI-2 is only concerned about active-tumor region. There were six tumor patients ($n = 6$), among the whole patient dataset used in this current study, with the presence of necrotic region. The APT-w contrast corresponding to the necrotic region for all types of normalizations was slightly lower than active tumor region. The APT_{Neg_NAWM} contrast (Type-4 normalization) was $3.51 \pm 2.1\%$

corresponding to the necrotic region of n = 6 patients; whereas, APT_{Neg_NAWM} contrast (Type-4 normalization) was 4.6 ± 1.61% in active tumor region corresponding to those n = 6 patients. Since APT-w values in necrotic tissue were slightly different than rest of tumor tissue and we had only six tumor patients; therefore, we did not exclude necrotic region from tumor during statistical analysis. In future, for a large number of data set having necrotic region, separate ROI analysis can be carried out for necrotic and rest of tumor tissue. Independent student's T-test and one-way ANOVA results showed that a greater number of histogram parameters of Type-4 normalization can differentiate neoplastic from infective mass lesions as well as among different groups of ICMLs than Type-3 normalizations. This shows that Type-4 normalization is better than Type-1,2,3 normalizations. Moreover, more histogram parameters corresponding to ROI-2 can differentiate neoplastic from infective mass lesions as well as among different categories of ICMLs than ROI-1. This shows that ROI analysis is better in ROI-2 than ROI-1. Histogram parameters viz. standard-deviation, median, mean of top percentiles provided improved differentiation between neoplastic and infective mass lesions compared to mean APT-w contrast. Histogram parameters like mean, SD, median, mode, mtop10, mtop25, mtop50, mtop75 and mtop90 are lower in LGG than HGG indicating higher severity in HGG. Histogram profile for HGG patients has been shifted towards right than histogram profile for LGG patients due to a higher mode. The current work studies the distribution of histogram profile of APT-w contrast and it showed that neoplastic mass lesion has negative skewness while infective mass lesion has positive skewness. The sample data set for each group of ICMLs was little skewed and kurtotic but it followed a normal distribution. FWHM of HGG is more than LGG, which also indicates that APT-w contrast of HGG is more diverged or heterogeneous. Thus, we assessed the usefulness of different histogram parameters and normalizations in predicting and differentiating ICMLs.

Previous studies [7] showed that APT-w MRI provides additional information about tumors than conventional MRIs. The present study also reveals that there are some key advantages of APT-w MRI over conventional MRIs. Firstly, sometimes PCT_1-w images fail to enhance the lesion region whereas APT map clearly shows well defined region of hyper-intensity (higher APT-w contrast) in the lesion region [10]. Secondly, T_2-w images can detect lesions but differentiation between active-tumor region and necrotic or cystic region is difficult, whereas, APT-w MRI can clearly differentiate necrotic region from active-tumor region [32].

The current study uses asymmetry analysis based on various normalization techniques for computing APT-w contrast which has confounding effects from MT and rNOE. Recently, alternative z-spectra fitting based approaches [37–39] are being developed for separating these effects, particularly at ultra-high fields. Recently, relaxation compensated APT effects [40] are being analyzed to mitigate these confounding effects. CEST and rNOE peaks are quite broad at 3T, therefore, further studies are required for robust z-spectra fitting.

There exist some limitations to the current study. Firstly, the number of patients, in each category of ICMLs were small. Secondly, in this study, APT-w contrast was only corrected for B_0 inhomogeneity. Due to time constraint at clinical scanner, B_1 inhomogeneity correction was not performed. As such B_1-field inhomogeneity in brain at 3T are quite small

(~10%) and should not affect the results of APT-w MRI substantially. Thirdly, in the current study, APT-w MRI data of a single representative slice was used. Three-Dimensional [1] APT-w imaging might improve the coverage of lesion, providing more information, and better signal-to-noise ratio (SNR).

Conclusion

The present study showed that APT-w contrast using Type-4 normalization and appropriate histogram parameters corresponding to ROI-2 provided better differentiation between neoplastic and infective mass lesions as well as among different group of ICMLs. Thus, APT_{Neg_NAWM} (Type-4 normalization) and active lesion region (ROI-2) should be used for studying APT-w MRI. APT-w MRI can be a promising tool in clinical settings for differentiating infective and neoplastic mass lesions as well as ICMLs in combination with other MRI techniques.

Supplementary Material

Refer to Web version on PubMed Central for supplementary material.

Acknowledgments

The authors acknowledge Philips India Limited for technical support in MRI data acquisition. The authors thank Dr. Jinyuan Zhou, Dr. Peter C.M. Van Zijl and Dr. Indrajit Saha for APT sequence and Dr. Mamta Gupta for editing manuscript. The authors also thank Dr. Sunita Ahlawat and Dr. Rana Patir for pathological information. This work was supported by MATRICS scheme, Science and Engineering Research Board, Department of Science and Technology (SERB-DST) Grant number: MTR_2017_001021 for overall study; National Institutes of Health (NIH) grants P41 EB015909 for APT pulse sequence.

References:

1. Zhao X, Wen Z, Zhang G, et al. (2013) Three-dimensional turbo-spin-echo amide proton transfer MR imaging at 3-tesla and its application to high-grade human brain tumors. Mol Imaging Biol 15:114–122 [PubMed: 22644987]
2. Sherry AD, Woods M (2009) Chemical exchange saturation transfer contrast agents for magnetic resonance imaging. Annu Rev Biomed Eng 10:391–411
3. Vinogradov E, Sherry AD, Lenkinski RE (2013) CEST: From basic principles to applications, challenges and opportunities. J Magn Reson 229:155–172 [PubMed: 23273841]
4. Liu G, Song X, Chan KWY, Mcmahon MT (2013) Nuts and bolts of chemical exchange saturation transfer MRI. NMR Biomed 26:810–828 [PubMed: 23303716]
5. Ward KM, Aletras AH, Balaban RS (2000) A New Class of Contrast Agents for MRI Based on Proton Chemical Exchange Dependent Saturation Transfer (CEST). J Magn Reson 143:79–87 [PubMed: 10698648]
6. Van Zijl PCM, Yadav NN (2012) Chemical Exchange Saturation Transfer (CEST): what is in a name and what isn't? Magn Reson Med 65:927–948
7. Zhou J, Lal B, Wilson DA, et al. (2003) Amide Proton Transfer (APT) Contrast for Imaging of Brain Tumors. Magn Reson Med 50:1120–1126 [PubMed: 14648559]
8. Zhou J, Payen JF, Wilson DA et al. (2003) Using the amide proton signals of intracellular proteins and peptides to detect pH effects in MRI. Nat Med 9:1085–1090 [PubMed: 12872167]
9. Zhou J, Yan K, Zhu H (2008) A simple model for understanding the origin of the amide proton transfer MRI signal in tissue. Magn Reson Med 45:788–802
10. Zhou J, Heo H, Knutsson L, et al. (2019) APT-Weighted MRI: Techniques, Current Neuro Applications, and Challenging Issues. J Magn Reson Imaging 1–18

11. Wen Z, Hu S, Huang F, et al. (2010) MR imaging of high-grade brain tumors using endogenous protein and peptide-based contrast. NeuroImage 51:616–622 [PubMed: 20188197]
12. Sun PZ, Cheung J, Wang E, Lo E (2011) Association between pH-weighted endogenous amide proton chemical exchange saturation transfer MRI and tissue lactic acidosis during acute ischemic stroke. J Cereb Blood Flow Metab 31:1743–1750 [PubMed: 21386856]
13. Sun PZ, Murata Y, Lu J, et al. (2008) Relaxation-compensated fast multislice amide proton transfer (APT) imaging of acute ischemic stroke. Magn Reson Med 59:1175–1182 [PubMed: 18429031]
14. Jiang S, Yu H, Wang X, et al. (2016) Molecular MRI differentiation between primary central nervous system lymphomas and high-grade gliomas using endogenous protein-based amide proton transfer MR imaging at 3 Tesla. J Eur Radiol 64–71
15. Togao O, Yoshiura T, Keupp J, et al. (2014) Amide proton transfer imaging of adult diffuse gliomas: Correlation with histopathological grades. Neuro Oncol 16:441–448 [PubMed: 24305718]
16. Jones CK, Schlosser MJ, Van Zijl PCM, et al. (2006) Amide proton transfer imaging of human brain tumors at 3T. Magn Reson Med 56:585–592 [PubMed: 16892186]
17. Debnath A, Gupta RK, Singh A (2016) APT MRI of intracranial Mass Lesions at 3T and comparison with perfusion parameters [abstract]. Proc. Intl. Soc. Mag. Reson. Med. Singapore
18. Togao O, Hiwatashi A, Yamashita K, et al. (2017) Grading diffuse gliomas without intense contrast enhancement by amide proton transfer MR imaging: comparisons with diffusion and perfusion-weighted imaging. Eur Radiol 27:578–588 [PubMed: 27003139]
19. Sakata A, Okada T, Yamamoto A, et al. (2015) Grading glial tumors with amide proton transfer MR imaging: different analytical approaches. J Neurooncol 122:339–348 [PubMed: 25559689]
20. Bai Y, Lin Y, Zhang W, et al. (2015) Noninvasive amide proton transfer magnetic resonance imaging in evaluating the grading and cellularity of gliomas. Oncotarget 8:5834–5842
21. Law M, Yang S, Wang H, et al. (2003) Glioma Grading: Sensitivity, Specificity, and Predictive Values of Perfusion MR Imaging and Proton MR Spectroscopic Imaging Compared with Conventional MR Imaging. Am J Neuroradiol 24:1989–1998 [PubMed: 14625221]
22. Singh A, Cai K, Haris M, et al. (2013) On B 1 inhomogeneity correction of in vivo human brain glutamate chemical exchange saturation transfer contrast at 7T. Magn Reson Med 69:818–824 [PubMed: 22511396]
23. Kang Y, Choi SH, Kim KG (2011) Gliomas: Histogram Analysis of Apparent Diffusion Coeffi cient Maps with Standard- or High- b -Value Diffusion-weighted MR Imaging—Correlation with Tumor Grade. Neuroradiology 261:882–890
24. Law M, Young R, Babb J, et al. (2007) Histogram analysis versus region of interest analysis of dynamic susceptibility contrast perfusion MR imaging data in the grading of cerebral gliomas. Am J Neuroradiol 28:761–766 [PubMed: 17416835]
25. Just N (2014) Improving tumour heterogeneity MRI assessment with histograms. Br J Cancer 111:2205–2213 [PubMed: 25268373]
26. Tee YK, Donahue MJ, Harston GWJ, et al. (2013) Quantification of amide proton transfer effect pre-And post-gadolinium contrast agent administration. J Magn Reson Imaging 40:832–838 [PubMed: 24214526]
27. Zhu H, Jones CK, Van Zijl PCM, et al. (2010) Fast 3D chemical exchange saturation transfer (CEST) imaging of the human brain. Magn Reson Med 64:638–644 [PubMed: 20632402]
28. Zhou J, Zhu H, Lim M, et al. (2013) Three-dimensional amide proton transfer MR imaging of gliomas: Initial experience and comparison with gadolinium enhancement. J Magn Reson Imaging 38:1119–1128 [PubMed: 23440878]
29. Kim M, Gillen J, Landman BA, et al. (2009) Water saturation shift referencing (WASSR) for chemical exchange saturation transfer (CEST) experiments. Magn Reson Med 61:1441–1450 [PubMed: 19358232]
30. Zaiss M, Schmitt B, Bachert P (2011) Quantitative separation of CEST effect from magnetization transfer and spillover effects by Lorentzian-line-fit analysis of z-spectra. J Magn Reson 211:149–155 [PubMed: 21641247]
31. Mehnert A, Jackway P (1997) An improved seeded region growing algorithm. Pattern Recognition Letters 18:1065–1071

32. Zhou J, Tryggestad E, Wen Z, et al. (2011) Differentiation between glioma and radiation necrosis using molecular magnetic resonance imaging of endogenous proteins and peptides. Nat Med 17:130–134 [PubMed: 21170048]
33. Park JE, Kim HS, Park KJ, et al. (2016) Pre and Posttreatment Glioma: Comparison of Amide Proton Transfer Imaging with MR Spectroscopy for Biomarkers of Tumor Proliferation. Radiology 278:514–523 [PubMed: 26491847]
34. Debnath A, Gupta RK, Singh A (2019) To evaluate the role of APT-w contrast, optimized for normalization and ROIs selection, in differentiating Infective and Neo-plastic Mass Lesions [abstract]. Proc. Intl. Soc. Mag. Reson. Med. Canada
35. Jiang S, Zou T, Eberhart CG, et al. (2017) Predicting IDH mutation status in grade II gliomas using amide proton transfer-weighted (APTw) MRI. Mag Reson Med 78:1100–1109
36. Yu H, Wen X, Wu P, et al. (2019) Can amide proton transfer–weighted imaging differentiate tumor grade and predict Ki-67 proliferation status of meningioma? Eur Radiol 18:1–9
37. Cai K, Singh A, Popatni H, et al. (2015) CEST signal at 2ppm (CEST@2ppm) from Z-Spectral fitting correlates with creatine distribution in brain tumor. NMR Biomed 28:1–8 [PubMed: 25295758]
38. Debnath A, Gupta RK, Singh A (2017) Lorentzian probabilistic sum based Z-spectrm fitting approach for computing CEST and NOE contrast and its comparison with lorentzian sum and asymmetry analysis. [abstract]. Proc. Intl Soc Mag Reson Med Hawaii, USA
39. Zaiss M, Xu LZ, Goerke S, et al. (2014) Inverse Z-spectrum analysis for spillover, MT and T1-corrected steady-state pulsed CEST-MRI-application to pH-weighted MRI of acute stroke. NMR Biomed 27:240–252 [PubMed: 24395553]
40. Goerke S, Soehngen Y, Deshmane A, et al. (2019) Relaxation-compensated APT and rNOE CEST-MRI of human brain tumors at 3T. Magn Reson Med 00:1–11

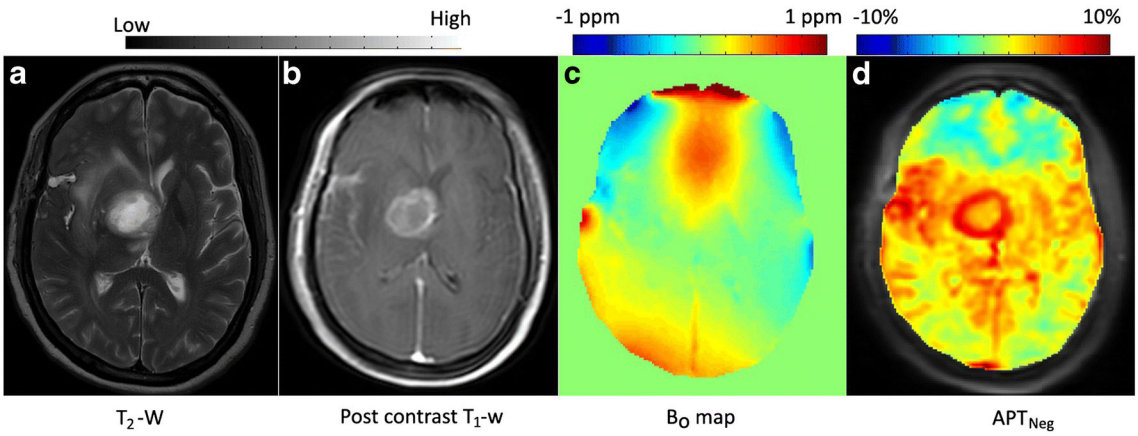

Figure 1.

A representative case of intra-cranial mass lesions (ICMLs). **a** T_2-weighted (w), **b** post contrast T_1-w image, **c** B_0 map and **d** APT_{Neg} map. Active region of lesion show hyper-intense APT-w contrast compared to contra-lateral region and other portion of the brain slice. Necrotic region of the lesion has lower APT-w contrast compared to active-tumor.

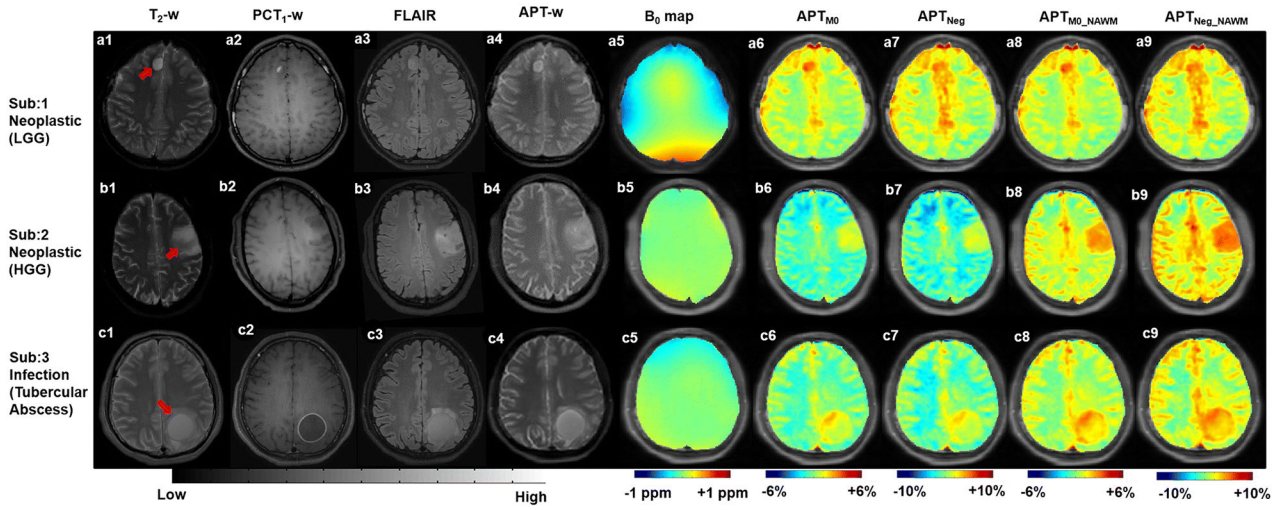

Figure 2.

Row 1–3 show MRI images of representative neoplastic mass lesion (low grade glioma (LGG) and high grade glioma (HGG)) and infective mass lesion (tubercular abscess) respectively. Column 1–9 contain T_2-weighted(w), post contrast T_1-w (PCT_1-w), FLAIR, APT-w images; B_0 map, APT_{M0}, APT_{Neg}, APT_{M0_NAWM} and APT_{Neg_NAWM} maps respectively. APT_{M0_NAWM} (Type-3) and APT_{Neg_NAWM} (Type-4) noramlizations reduces the variability between NAWM and NAGM than APT_{M0} (Type-1) and APT_{Neg} (Type-2) noramlizations. Red arrows point to lesion region.

Abbreviation: NAWM – normal appearing white matter; NAGM – normal appearing gray matter.

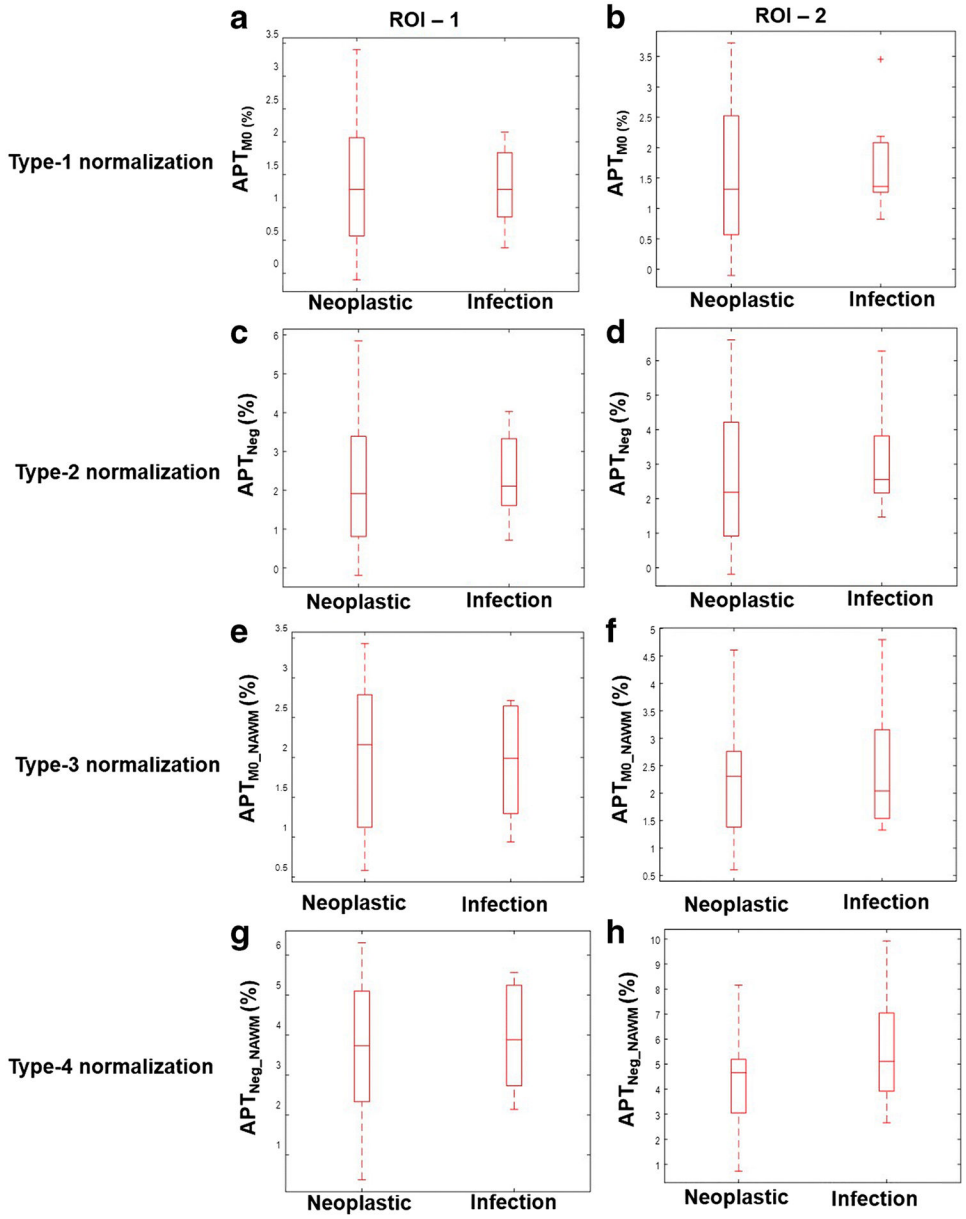

Figure 3.

Box and whisker plots show quantitative comparison of neoplastic and infective mass lesions for all types of APT-w contrast normalizations corresponding to two ROIs. ROI-1 represents entire lesion and ROI-2 is active-lesion region. Type-1, Type-2, Type-3 and Type-4 normalizations represents APT_{M0}, APT_{Neg}, APT_{M0_NAWM} and APT_{Neg_NAWM} contrast respectively. Different range of scale was used for different normalizations to obtain better representation and visualization of individual plots. Abbreviation: APT-w – amide proton transfer weighted; ROI – region of interest.

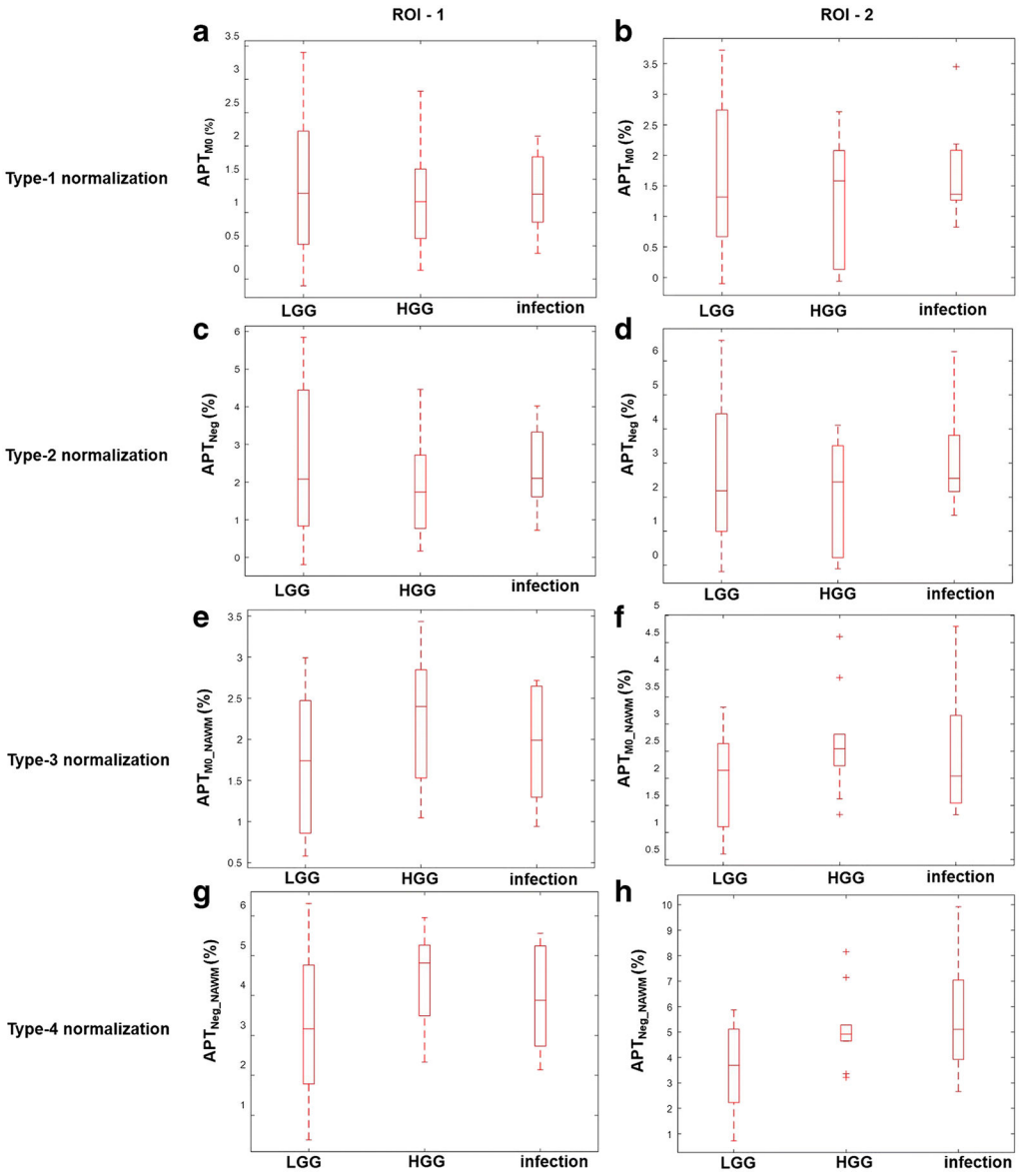

Figure 4.

Box and whisker plots show quantitative comparison of different types APT-w contrast normalizations among different groups of ICMLs for two ROIs. ROI-1 represents entire lesion and ROI-2 is active-lesion region. Type-1, Type-2, Type-3 and Type-4 normalizations represents APT_{M0}, APT_{Neg}, APT_{M0_NAWM} and APT_{Neg_NAWM} contrast respectively. Different range of scale was used for different normalizations to obtain better representation and visualization of individual plots. Abbreviation: APT-w – amide proton transfer weighted; ROI – region of interest; LGG – low grade glioma; HGG – high grade glioma.

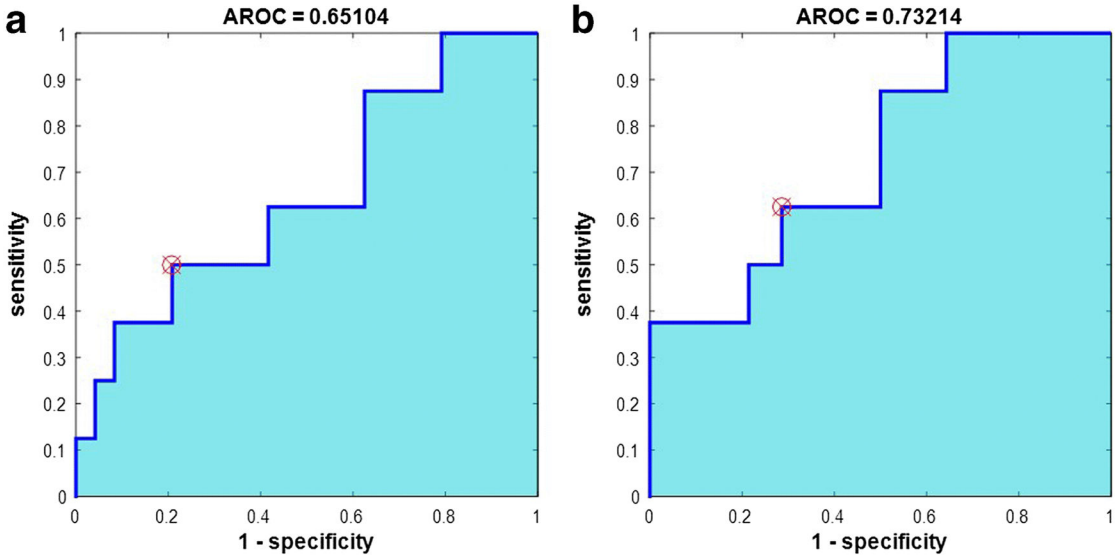

Figure 5.

ROC analysis of mean APT_{Neg_NAWM}-w contrast (Type-4 normalizations) corresponding to ROI-2 for differentiation between **a** neoplastic and infective mass lesion and between **b** low grade glioma and infective mass lesion. Abbreviation: AROC – area under curve for ROC plot.

Table 1.

Histogram parameters of Type-3 and Type-4 normalizations, corresponding to ROI-1 and ROI-2, which provide significance difference ($p < 0.05$), using T-test, between neoplastic and infective mass lesions.

	ROI-1		ROI-2	
	Histogram Parameters	**p value (T-test)**	**Histogram parameters**	**p value (T-test)**
Type-3 normalization	skewness	0.03	kurtosis	0.04
	sdtop50	0.03	entropy	0.05
	sdtop75	0.03	FWHM	0.03
Type-4 normalization	skewness	0.03	mean	0.05
	sdtoplO	0.05	SD	0.02
	sdtop25	0.03	kurtosis	0.04
	sdtop50	0.0l	mtop50	0.05
	sdtop90	0.0l	mtop75	0.04
			mtop90	0.04
			sdtop10	0.03
			sdtop25	0.01

Table 2.

Histogram parameters of Type-3 and Type-4 normalizations, corresponding to ROI-1 and ROI-2, which provide significance difference ($p < 0.05$), using One-way ANOVA, between different groups of intra cranial mass lesions.

	ROI-1			ROI-2		
	Histogram parameters	**p value (ANOVA)**	**p value (post hoc)**	**Histogram parameters**	**p value (ANOVA)**	**p value (post hoc)**
Type-3 normalization	skewness	0.06	0.05[c]	mtop50	0.04	0.06[b]
	sdtoplO	0.05	0.05[b]	mtop75	0.03	0.05[b]
	sdtop50	0.05	0.04[b]	mtop90	0.03	0.06[b]
	sdtop75	0.06	0.05[b]			
Type-4 normalization	sdtop25	0.04	0.03[b]	mean	0.03	0.04[b]
	sdtop50	0.02	0.01[b]	SD	0.05	0.04[b]
	sdtop75	0.02	0.0l[b]	median	0.03	0.05[b]
				mode	0.02	0.04[a]
				mtop10	0.03	0.04[b]
				mtop25	0.02	0.03[b]
				mtop50	0.01	0.02[b]
				mtop75	0.01	0.01[b]
				mtop90	0.01	0.01[b]
				sdtop25	0.03	0.03[b]

[a] $p < 0.05$ between low grade glioma (LGG) and high grade glioma (HGG)

[b] $p < 0.05$ between low grade glioma (LGG) and infection

[c] $p < 0.05$ between high grade glioma (HGG) and infection

Table 3.

ROC analysis of Type-4 normalized APT-w contrast corresponding to ROI-2 for differentiating neoplastic from infective mass lesions.

HP	p value	Sensitivity (%)	Specificity (%)	AUC (lb, ub) (%)	cut-off (%)	Accuracy (%)
mean	0.05	50	80	65(42, 88)	5.3	72
SD	0.02	62.5	58.3	67(42, 92)	0.69	84.37
kurtosis	0.04	25	67	27(4, 48)	2.87	56.25
mtop50	0.05	75	58.3	68(47, 90)	5.29	62.5
mtop75	0.04	75	62.5	70(47, 91)	5.81	65.62
mtop90	0.04	75	58.3	68(46, 91)	5.98	62.5
sdtop10	0.03	62.5	70.8	66(41, 91)	0.71	68.75
sdtop25	0.01	62.5	75	68.23(42, 95)	0.64	71.88

AUC – area under curve;

lb and ub are lower and upper bound with 95% confidence interval;

HP -histogram parameters

Table 4.

ROC analysis of Type-4 normalized APT-w contrast corresponding to ROI-2 to differentiate low grade glioma (LGG) and infective mass lesions.

HP	p value (post hoc)	Sensitivity (%)	Specificity (%)	AUC (lb, ub) (%)	cut-off (%)	Accuracy (%)
mean	0.04	62.5	71.43	73.21(51, 95)	4.77	68.18
SD	0.04	87.5	50	71.4(46, 96)	0.58	81.81
median	0.05	62.5	71.43	74.1(53, 95)	4.68	68.18
mtop10	0.04	62.5	71.43	73.2(51, 95)	4.39	68.18
mtop25	0.03	87.5	57.14	75(54, 96)	4.46	68.18
mtop50	0.02	75	71.43	76.8(56, 97)	5.21	72.72
mtop75	0.01	75	71.43	75.9(55, 96)	5.60	72.72
mtop90	0.01	75	71.43	75(53, 96)	5.78	72.72
sdtop25	0.03	62.5	78.57	71.4(45, 97)	0.64	72.72

AUC – area under curve;

lb and ub are lower and upper bound with 95% confidence interval;

HP -histogram parameters